Out-of-plane Electrode Architecture for Fused Silica Micro-glassblown 3-D Wineglass Resonators

Doruk Senkal, Mohammed J. Ahamed, Mohammad H. Asadian, Sina Askari, and Andrei M. Shkel
MicroSystems Laboratory, Mechanical and Aerospace Engineering
University of California, Irvine
Irvine, CA, USA 92697
E-mail: {dsenkal, mahamed, asadianm, ashkel}@uci.edu

***Abstract*—In this paper, we report an out-of-plane electrode architecture for micro-glassblown fused silica wineglass gyroscopes. Transduction is enabled by the 3-D mode shape of the wineglass resonator, which allows one to drive and sense the wineglass modes using the out-of-plane component of the vibratory motion. The transduction architecture has been succesfully demonstrated on fused silica wineglass resonators with Q-factor over 1 million, on both modes, and high frequency symmetry ($\Delta f/f$) of 132 ppm at a compact size of 7 mm diameter and center frequency of 105 kHz. Out-of-plane electrode architecture enables the use of sacrifical layers to define the capacitive gaps, which enables wafer-level integration, mitigates alignment issues and provides uniformly small gaps. 10 μm capacitive gaps have been demonstrated on a 7 mm shell, resulting in over 9 pF of active capacitance within the device. Wafer-level scalability of out-of-plane electrode architecture may enable batch-fabrication of high performance fused silica micro-glassblown wineglass gyroscopes at a significantly lower cost than their precision-machined macro-scale counterparts.**

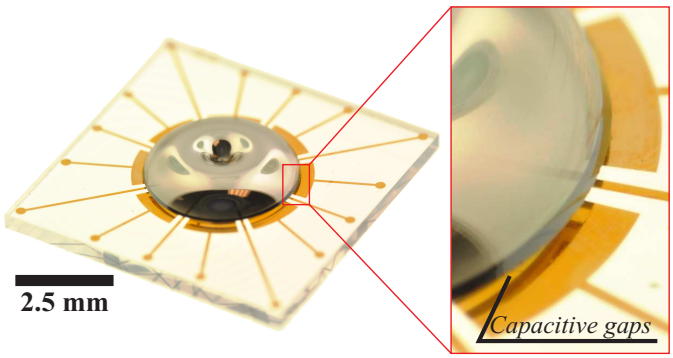

Fig. 1. Micro-glassblown fused silica wineglass resonator on out-of-plane electrodes. The die is transparent as the entire device is made out-of-fused silica. Diameter of this particular device is 4 mm.

I. Introduction

There is an interest in 3-D MEMS wineglass resonator architectures for use in next-generation inertial sensing applications due to potential advantages in symmetry, minimization of energy losses, immunity to external vibrations and die stresses [1]–[5].

With the emergence of new 3-D micro-machining techniques, batch fabrication of 3-D MEMS wineglass structures is becoming feasible. Primarily, two main methods are employed in fabrication of MEMS wineglass structures: (1) deposition of thin-films on pre-defined molds, and (2) glass-blowing the device layer into a pre-defined cavities. For example, Q-factor of 19.1k have been demonstrated on poly-silicon shell structures deposited in pre-etched cavities [1]. Q-factors up to 24k [2] were measured on poly-diamond wineglass shells deposited in pre-etched cavities and up to 20k were measured on sputtered ultra low expansion (ULE) glass shells deposited on precision ball lenses [3]. Q-factors as high as 7.8k was demonstrated on blow-molded bulk metallic glass shells [4] and 1 million on fused silica shells [5].

In micro-machined wineglass gyrocopes the main focus of research remains to be Q-factor and frequency symmetry (Δf), as they directly relate to gyro performance metrics, such as rate sensitivity, noise performance, and power consumption. However, defining electrodes on these 3-D MEMS structures with sufficiently small gaps and uniformity provides an additional challenge for gyroscope operation. For thin film devices this is accomplished by defining electrode structures within the pre-etched cavity by placing a sacrificial layer in between [2], [6]. For glassblown devices a wide variety architectures have been demonstrated, including deep glass dry etching of the capacitive gaps [7] ($> 30\mu$m), utilization of thermal mismatch between the shell and the mold to create the capacitive gaps [4] ($\sim$ 15μm), and various assembly techniques [8], [9] ($\sim 15\mu$m). Despite these advances, factors such as misalignment errors between the shell and the electrodes, cross-talk between electrodes, relatively large gaps on assembly based techniques and lack of scalability remain to be a challenge.

In this paper, we explore an alternative electrode architecture, in conjunction with the fused silica micro-glassblowing paradigm. Micro-glassblowing process relies on viscous deformation of the device layer under the influence of surface tension and pressure difference between inner and outer sides of the device layer to define the 3-D shell structure, as opposed to conventional deposition, molding, or etching techniques. This leads to levels of smoothness and structural symmetry that is not available through conventional fabrication techniques. In addition, micro-glassblowing allows the use of low internal loss, isotropic fused silica material on a wafer-level without the need for challenging dry etching techniques [10]. However, the 3-D wineglass structure brings forth challenges for electrode integration, due to the high aspect ratio, aspherical resonator element and high temperature fabrication process (1700 °C). To address these challenges we propose an out-of-plane electrode architecture. Transduction is enabled by detecting and driving

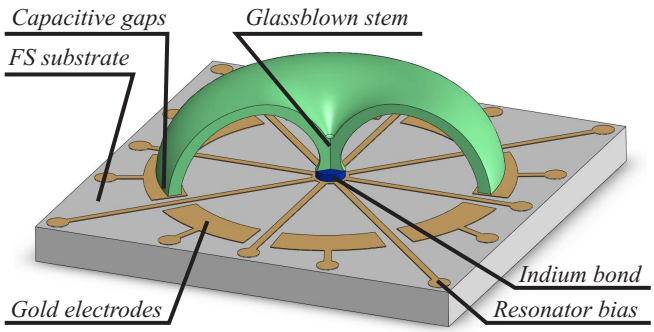

Fig. 2. Out-of-plane electrode architecture consists of a micro-glassblown fused silica wineglass resonator and planar Cr/Au electrodes on fused silica.

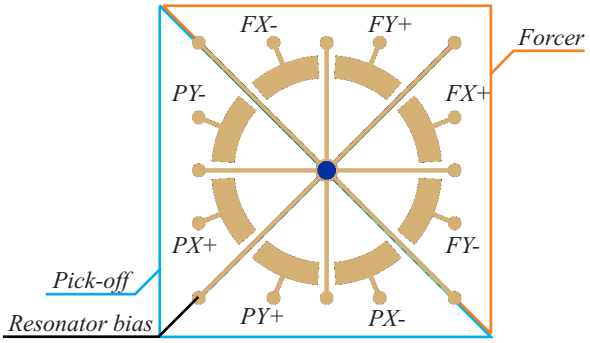

Fig. 3. Electrode configuration used in this paper. 4 electrodes are designated as forcer (FX and FY) and 4 are designated as pick-off (PX and PY). Both the forcer and pick-off channels have differential pairs (i.e. FX+ and FX-).

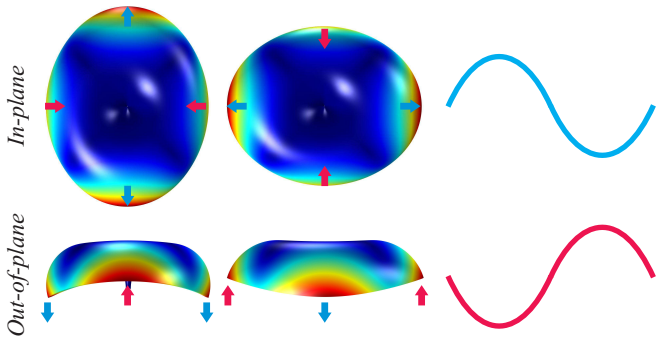

Fig. 4. Out-of-plane transduction scheme utilizes out-of-plane component of wineglass modes to drive and sense in-plane motion.

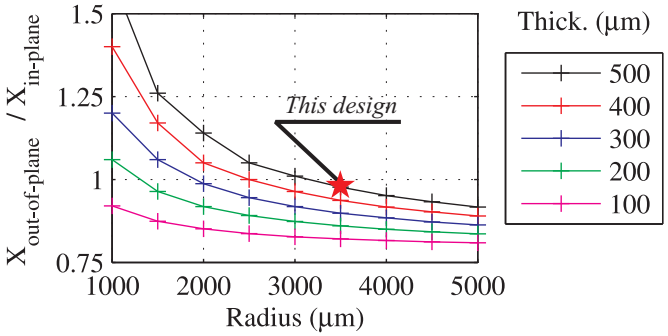

Fig. 5. Out-of-plane to in-plane displacement ratio for mushroom resonators: Due to the 3-D nature of the resonator, the ratio is close to 1:1. Star marks the design presented in this paper.

the spatial modes of the 3-D wineglass resonator, which allows one to drive and sense the wineglass modes using their out-of-plane components.

Micro-glassblowing of borosilicate glass spherical shell structures have been demonstrated for nuclear magnetic resonance applications [11]. Later, fused silica and ultra low expansion glass micro-glassblowing of inverted-wineglass structures have been demonstrated at temperatures as high as 1700 °C [12]. Assembled electrode structures [9], as well as deep glass dry etched electrode structures have been developed for electrostatic transduction of micro-glassblown structures [7], [10]. Finite element analysis of the micro-glassblowing process [13], and further improvement in the fabrication process led to frequency splits (Δf) as low as 0.16 Hz on borosilicate glass wineglass structures [7].

In this work, we report the most recent developments in the out-of-plane electrode architecture, resulting in uniform 10 μm capacitive gaps on a 7 mm shell, resulting in over 9 pF of active capacitance within the device. In addition, Q-factors as high as 1 million have been demonstrated on fused silica wineglass resonators at 7 mm diameter [14].

II. Design

Wineglass coriolis vibratory gyroscopes typically utilize 8 to 32 electrodes to drive and sense the primary (n = 2) wineglass modes. High aspect ratio 3-D wineglass geometry makes it challenging to fabricate radial electrodes with small and uniform capacitive gaps. Deep glass etching techniques typically result in large capacitive gaps [7], whereas post-fabrication assembly techniques [5], [9], are susceptible to mis-alignment errors and create a bottle-neck in batch-fabrication of the devices at wafer level.

In this paper, we explore an alternative transduction paradigm based on out-of-plane electrode architecture. The electrode architecture consists of a micro-glassblown fused silica wineglass resonator and planar Cr/Au electrodes defined on a fused silica substrate, Fig. 2. Out-of-plane capacitive gaps are formed between the Cr/Au metal traces and the perimeter of the wineglass resonator. Electrostatic transduction is made possible by the 3-D mode shape of the wineglass resonator: in-plane deformation of wineglass modes is accompanied by an out-of-plane deformation, Fig. 4. This permits the use of out-of-plane transduction to drive and sense the in-plane oscillations, which are sensitive to Coriolis forces along the z-axis of the structure [15].

In our implementation, a total of 8 electrodes are used, which is the minimal configuration to drive and sense the n = 2 wineglass modes. 4 electrodes are designated as forcer (FX and FY) and 4 are designated as pick-off (PX and PY). Both the forcer and pick-off channels have differential pairs (i.e. FX+ and FX-). The resonator is biased using any of the 8 traces that extend from the central anchor point. These traces also help suppress parasitic coupling between adjacent electrodes by sinking stray currents.

As the thickness of the shell limites the maximum surface area for the out-of-plane electrodes, typically a smaller surface

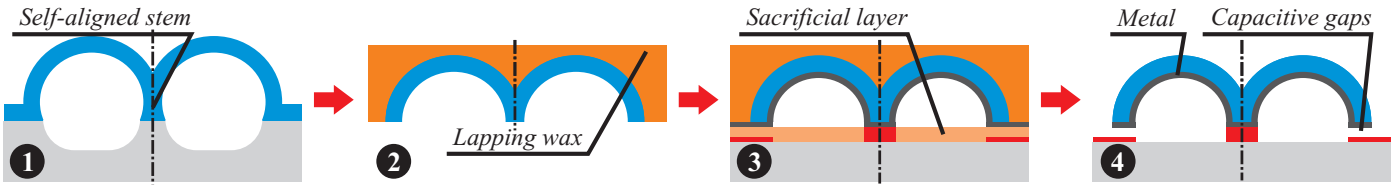

Fig. 6. Wafer-level fabrication process for fused silica micro-wineglass structures.

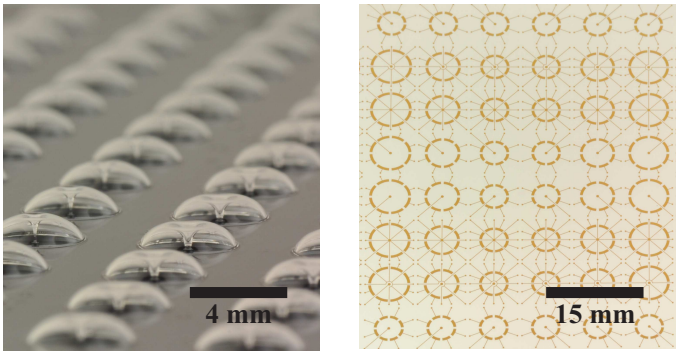

Fig. 7. Array of micro-glassblown wineglass structures (left), array of out-ot-plane electrodes on a fused silica wafer (right).

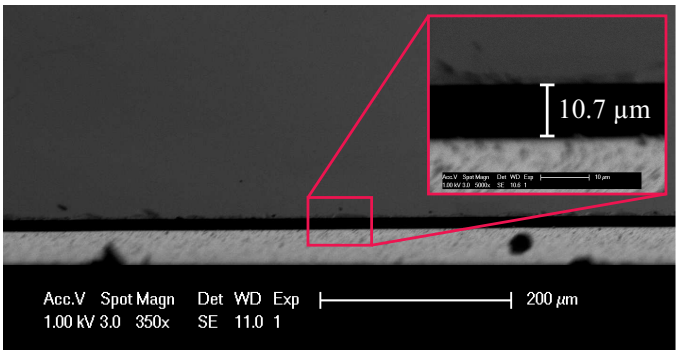

Fig. 8. Uniform 10 μm capacitive gaps have been demonstrated on 7 mm shell structures, resulting in over 9 pF total active capacitance on the device.

area is utilized for capacitive gaps compared to radial electrodes. However, this is offset by the fact that planar nature of the electrode structure, which makes it easier to obtain smaller capacitive gaps, which helps compensate for the loss of surface area. In addition, sacrificial layers and wafer-to-wafer bonding techniques can be used to define the capacitive gaps, which makes the process very robust to alignment errors, as the gap uniformity is defined by the thickness of the sacrificial layer and not by the wafer to resonator alignment accuracy. Finally, the metal traces for the electrodes can be defined on the same material used for the resonator (i.e. fused silica), providing uniform coefficient of thermal expansion between the electrode die and the resonator.

Another important parameter to consider is the ratio of out-of-plane motion to in-plane motion, which indicates the transduction efficiency of the out-of-plane electrodes. Finite element modeling using Comsol Multiphysics package revealed that, for mushroom type geometries the ratio of out-of-plane motion to in-plane motion is close to 1:1, leading to very efficient out-of-plane transduction, Fig. 5.

III. Fabrication

Fabrication process utilizes two wafers: a wineglass shell wafer and an electrode wafer, Fig. 7. Fabrication process starts with LPCVD poly-silicon deposition on 1 mm thick fused silica wafers of up to $\sim 2\mu$m thickness. The poly-silicon mask is later patterned lithographically and is used to etch cavities into fused silica wafers down to $\sim$ 300 μm in depth. The next step of the fabrication process is plasma assisted fusion bonding of a 500 μm thick fused silica device layer (Corning 7980) [12]. The plasma assisted fusion bonding process for bonding fused silica wafer pairs can be summarized as follows:

1) Cleaning of the wafer pair using solvent and RCA clean,
2) Plasma activation using oxygen plasma (50 Watts power for 2 minutes, 24 sccm O2 flow),
3) DI water rinse followed by N2 dry,
4) Optical contacting of the activated surfaces,
5) Room temperature anneal for $>$ 48 hours,
6) Curing the wafer stack at 400 °C for 6 hours.

The bond creates a seamless hermetic seal around the etched cavities without using any intermediate material. The glassblowing is performed at 1700 °C for $\sim$ 2 minutes and rapidly cooled to room temperature, Fig 6(a). During glassblowing the device layer at the central post merges to create a solid, self-aligned stem structure, critical for high-Q operation. Shells are released by back-lapping the wafer stack to release using an Allied Multiprep 12" lapping system, Fig 6(b). A series of diamond lapping films with descending grit size of 30 μm $\Rightarrow$ 6 μm $\Rightarrow$ 3 μm $\Rightarrow$ 1 μm $\Rightarrow$ 0.5 μm $\Rightarrow$ 0.1 μm are used for lapping, followed by final polish using 50 nm colloidal suspension and polishing cloth. Interior surface of the wineglasses is metallized with 50 nm thick sputtered Iridium. Only the interior surface is metallized to minimize the influence of the metal film on the shell resonator. Metallization is performed on a two axis planetary stage for film uniformity, in which the wafer is continuously rotated along z-axis and oscillated $\pm 15°$ along x-axis.

Fused silica out-of-plane electrode structures are fabricated on a seperate wafer by blanket coating with Cr/Au (100 nm / 500 nm), spinning a thin layer of photo-resist sacrificial layer and patterning the Cr/Au features using etch-back. In this process, the photoresist is used both to pattern the electrodes and as a sacrificial layer to create the capacitive gaps. Subsequently, lapped and metalized wineglass wafer is bonded to

the out-of-plane electrode wafer at the stem of each wineglass using low out-gassing epoxy, Ablebond JM7000 or Indium, Fig 6(c). Once the bonding is complete, the sacrificial layer is removed to release the inverted wineglass structures around their perimeter, Fig 6(d), creating capacitive gaps between the metalized inverted wineglass structures and the Cr/Au electrodes, Fig 8.

IV. Experimental Results

Capacitive gaps as low as 10 μm on a 7 mm shell have been demonstrated, resulting in over 9 pF of total active capacitance within the device. Frequency sweep using out-of-plane electrodes revealed Q-factor of 1.14 million and frequency split of 14 Hz at a center frequency of 105 kHz ($\Delta f/f$ = 132 ppm), Fig. 9.

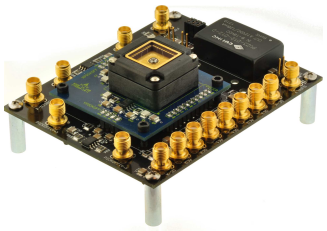

(a) Front-end electronics

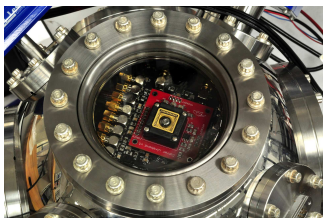

(b) Vacuum chamber setup

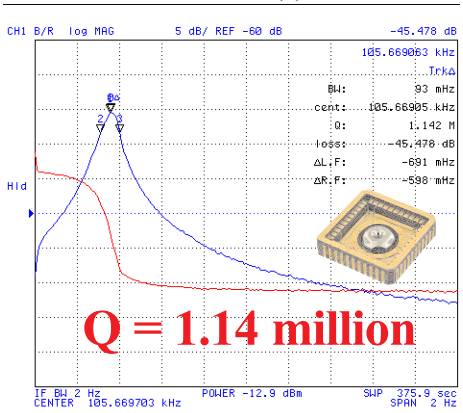

(c) Electrostatic frequency sweep from out-of-plane electrodes.

Fig. 9. Frequency sweep revealed a Q-factor of 1.14 million and as fabricated freq. split (Δf) of 14 Hz at 105 kHz center freq.

V. Conclusions

Out-of-plane capacitive transduction on MEMS wineglass resonators with 10 μm capacitive gaps have been demonstrated for the first time. Electrostatic characterization of wineglass resonators using out-of-plane electrodes revealed Q-factors over 1 million, on both principle directions of n = 2 modes, and high frequency symmetry ($\Delta f/f$) of 132 ppm at 105 kHz center frequency and at a size of 7 mm diameter, Table I.

Wafer-level scalability of out-of-plane electrode architecture may enable batch-fabrication of high performance fused silica micro-glassblown wineglass gyroscopes at a significantly lower cost than their precision-machined macro-scale counterparts.

TABLE I. Summary of device parameters for a 7 mm fused silica wineglass resonator.

Shell diameter	7 mm
Shell thickness	$\sim 500\mu$m
Effective mass	8 μg
Quality factor	$>$ 1 million
Center frequency	105 kHz
Frequency split (Δf)	14 Hz
Total capacitance	9.7 pF
Total dC/dX	970 nF/m

Acknowledgment

This material is based upon work supported by DARPA grant W31P4Q-11-1-0006 (Program Manager Dr. Robert Lutwak).

References

[1] P. Shao, V. Tavassoli, L. Chang-Shun, L. Sorenson, and F. Ayazi, "Electrical characterization of ALD-coated silicon dioxide micro-hemispherical shell resonators," in *IEEE MEMS*, 2014, pp. 612–615.

[2] A. Heidari, M. Chan, H.-A. Yang, G. Jaramillo, P. Taheri-Tehrani, P. Fonda, H. Najar, K. Yamazaki, L. Lin, and D. A. Horsley, "Micromachined polycrystalline diamond hemispherical shell resonators," in *TRANSDUCERS*, Barcelona Spain, 2013, pp. 2415–2418.

[3] Y. Xie, H. C. Hsieh, P. Pai, H. Kim, M. Tabib-Azar, and C. H. Mastrangelo, "Precision curved micro hemispherical resonator shells fabricated by poached-egg micro-molding," in *IEEE Sensors*, Taipei, Taiwan, 2012, pp. 279–283.

[4] M. Kanik, P. Bordeenithikasem, J. Schroers, D. Kim, and R. T. M'Closkey, "Microscale Three-Dimensional Hemispherical Shell Resonators Fabricated from Metallic Glass," in *IEEE ISISS*, Laguna Beach, CA, 2014, pp. 9–12.

[5] J. Cho, J. Woo, J. Yan, R. L. Peterson, and K. Najafi, "A high-Q birdbath resonator gyroscope (BRG)," in *TRANSDUCERS*, no. June, 2013, pp. 1847–1850.

[6] L. D. Sorenson, X. Gao, and F. Ayazi, "3-D micromachined hemispherical shell resonators with integrated capacitive transducers," in *IEEE MEMS*, Jan. 2012, pp. 168–171.

[7] D. Senkal, M. J. Ahamed, A. Trusov, and A. M. Shkel, "Achieving Sub-Hz Frequency Symmetry in Micro-Glassblown Wineglass Resonators," *Journal of Microelectromechanical Systems*, vol. 23, no. 1, pp. 30–38, 2014.

[8] J. Cho, T. Nagourney, A. Darvishian, B. Shiari, J. Woo, and K. Najafi, "Fused silica micro birdbath shell resonators with 1.2 million Q and 43 second decay time constant," in *Hilton Head*, 2014, pp. 103–104.

[9] D. Senkal, M. J. Ahamed, A. Trusov, and A. M. Shkel, "Adaptable test-bed for characterization of micro-wineglass resonators," in *IEEE MEMS*, 2013, pp. 469–472.

[10] M. J. Ahamed, D. Senkal, A. A. Trusov, and A. M. Shkel, "Deep NLD plasma etching of fused silica and borosilicate glass," in *IEEE Sensors*, Baltimore, Maryland, USA, 2013, pp. 1767–1770.

[11] E. J. Eklund and A. M. Shkel, "Self-inflated micro-glass blowing," *US Patent 8,151,600*, 2012.

[12] D. Senkal, M. J. Ahamed, A. A. Trusov, and A. M. Shkel, "High temperature micro-glassblowing process demonstrated on fused quartz and ULE TSG," *Sensors and Actuators A: Physical*, vol. 201, pp. 525–531, Dec. 2012.

[13] D. Senkal, M. J. Ahamed, and A. M. Shkel, "Design and Modeling of Micro-glassblown Inverted-wineglass Structures," in *IEEE ISISS*, Laguna Beach, CA, 2014, pp. 13–16.

[14] D. Senkal, M. J. Ahamed, S. Askari, and A. M. Shkel, "1 million Q-factor demonstrated on micro-glassblown fused silica wineglass resonators with out-of-plane electrostatic transduction," in *Hilton Head*, 2014, pp. 68–71.

[15] A. Renault and P. Vandebeuque, "Hemispherical resonator with divided shield electrode," *US Patent 6,945,109*, 2005.